Journal of Materials Chemistry A

ROYAL SOCIETY OF CHEMISTRY

PAPER

View Article Online
View Journal | View Issue

Cite this: J. Mater. Chem. A, 2025, 13, 30224

Beyond vehicular transport: fluorination-induced structural diffusion in ether electrolytes

Sidhant Kumar Barik and Hemant Kumar*

Developing high-performance sodium-ion batteries requires stable electrolytes with high ionic conductivity and cation transference numbers. This study employs molecular dynamics simulations and analysis of Onsager transport coefficients to investigate the influence of fluorination on ion transport mechanisms in 1,2-diethoxyethane (DEE)-based electrolytes. We demonstrate that fluorination significantly alters the static and dynamic characteristics of the solvation environment, leading to distinct trends in conductivity and transference number. Low-fluorinated bilaterally substituted ethers exhibit low conductivity due to long solvent lifetimes and a predominantly vehicular transport mechanism. In contrast, highly fluorinated ethers, particularly F3F0/F3F3, demonstrate enhanced transport properties due to a shift toward structural diffusion facilitated by fast anion and solvent exchange dynamics. Despite increased ion pairing, high conductivity is achieved through concerted ion motion and ultrafast relaxation modes, surpassing the ionic conductivity of the nonfluorinated parent solvent. Our analysis reveals the crucial role of distinct ion correlations in highly aggregated systems and highlights the continuous ion pair lifetime as a key descriptor for understanding cation–anion correlations. These molecular-level insights provide a framework for the rational design of electrolytes with tailored transport properties, advancing the development of high-performance sodium-ion batteries.

Received 26th May 2025
Accepted 6th August 2025

DOI: 10.1039/d5ta04224k

rsc.li/materials-a

1 Introduction

Liquid electrolytes serve as a critical component in electrochemical devices, such as sodium-ion batteries (SIBs), enabling the transport of ions between electrodes during charge and discharge processes. The efficacy of this ionic transport is fundamentally governed by the solvation structure, the extent of ion pairing, and the underlying transport mechanisms, which, in turn, are modulated by thermodynamic variables, including salt concentration, solvent dielectric permittivity, and temperature.[1–6] In conventional dilute liquid electrolytes, cations typically exist as solvated complexes, wherein the ion is coordinated by a defined number of solvent molecules. The ionic transport in such systems is dominated by a vehicular mechanism, characterized by the translational diffusion of the entire solvated complex through the electrolyte medium.[7,8] However, recent investigations have increasingly focused on alternative transport pathways, particularly structural diffusion (or Grotthuss-like mechanism), wherein the ion undergoes a sequential transfer process between adjacent coordination sites within a more structured electrolyte environment.[9–13]

Studies suggest that shifting from a primarily vehicular mode of transport to a mixed vehicular-structural mode can improve ionic conductivity and transference numbers.[14,15] This hopping mechanism is often prominent in high-concentration electrolytes (HCEs) or weak-solvent electrolytes (WSEs), where the elevated salt concentration or reduced solvent-coordinating ability promotes the formation of extended ionic aggregates and networks.[16–19] A comprehensive understanding of the relative contributions of vehicular and structural diffusion to the overall ionic conductivity and the cation transference number is paramount for the rational design of electrolytes exhibiting enhanced transport properties. In this study, we demonstrate that strategic fluorination of the solvent molecules can be an effective molecule design approach to promote faster structural relaxation, thereby boosting structural diffusion and ultimately enhancing ion transport and cation transference number in SIBs.

Fluorinated solvents, due to their unique electronic properties, can alter the interactions between ions and solvent molecules, leading to changes in the solvation shell structure and ion transport behavior. Studies have shown that fluorination can mimic the behavior of HCEs/WSEs by promoting the formation of more structured electrolyte environments with reduced free solvent molecules.[20,21] For instance, fluorinated ethers, like those with $-CH_2F$, $-CHF_2$, or $-CF_3$ terminal groups, can reduce solvating power and promote anion clustering, similar to what is observed in HCEs.[22–25] This can facilitate structural diffusion, potentially improving the transference number and ionic conductivity. We focus on 1,2-diethoxyethane (DEE) as the backbone solvent, which has demonstrated enhanced high-

Department of Physics, School of Basic Sciences, Indian Institute of Technology Bhubaneswar, Argul, Odisha, 752050, India. E-mail: hemant@iitbbs.ac.in

voltage stability while improving Li metal coulombic efficiency.[26,27] By systematically fluorinating the terminal ends of DEE molecules, we study a series of fluorinated DEE (F-DEE) analogues with varying degrees of fluorination. By computing the Onsager coefficient from trajectories obtained using all-atom molecular dynamics (MD) simulations, we investigated the impact of fluorination on ion conduction properties. Our findings demonstrate a striking correlation between the degree of fluorination and the dominant ion transport mechanism. Highly fluorinated DEE analogues exhibit a remarkable enhancement in both the rate of structural relaxation and the contribution of structural diffusion to the overall Na^+ transport, leading to significantly improved diffusion coefficients and transference numbers. Further, by systematically analyzing the solvation structure around Na^+ ions and, crucially, the dynamics of solvation shell relaxation, we correlate faster ion transport with the structure of the solvation shell.

In less fluorinated DEE molecules, Na^+ ions are found to be mostly solvated by a smaller number of solvent molecules (typically three). As the degree of fluorination increases, the solvation number around Na^+ increases, with highly fluorinated DEE analogues exhibiting a solvation number of four. This seemingly subtle change in solvation structure profoundly impacts the system's dynamics. The larger, more populated solvation shell in the highly fluorinated solvents leads to enhanced structural relaxation, facilitating fast exchange of anion and solvent molecules within the first solvation shell, which in turn favors structural diffusion of Na^+. This results in a higher ionic conductivity and Na^+ transference number compared to the lower fluorinated counterparts.

This fluorination-induced enhancement of structural relaxation and the consequent shift in the dominant ion transport mechanism represents a key finding of this study. While previous research has highlighted the significance of fluorinated solvents in enhancing electrochemical stability, safety, and interfacial characteristics, it is acknowledged that fluorination reduces ionic diffusion for lithium-ion batteries.[22,23,25,27] However, our study demonstrates that fluorination can enhance ionic diffusion for certain fluorinations through accelerated structural diffusion and the optimization of solvation shell dynamics. Our results provide valuable molecular-level insights into the interplay between solvent structure, solvation dynamics, and ion transport mechanisms. By demonstrating that controlled fluorination can effectively promote structural diffusion, we open up new avenues for designing high-performance electrolytes with enhanced ionic conductivity and transference numbers.

2 Method

To investigate the solvation behavior, all-atom MD simulations were conducted using LAMMPS for electrolyte compositions resulting from the combination of every F-DEE solvent and NaFSI salt at a concentration of 1 M.[28] The details of the system for each solvent are given in Table S1. The OPLS-AA force field parameters for all F-DEE solvents were generated using the Ligpargen web server, while partial atomic charges were determined by fitting the molecular electrostatic potential at atomic centres in Gaussian16 using the *ab initio* B3LYP/6-311G level of theory.[29,30] Force field parameters for the Na^+ and FSI^- anions were obtained from Lopes with partial charges of +1 and −1, respectively.[29,31] The electrolyte systems were set up initially with the salt and solvent molecules distributed randomly in the simulation boxes using PackMol.[32] A non-bonded Lennard-Jones cutoff of 1.0 nm was applied, and long-range electrostatic interactions were treated using the particle–particle particle-mesh (PPPM) method with a real-space cutoff of 1.0 nm. Bonds involving hydrogen atoms were constrained using the SHAKE algorithm.[33] For each system, an initial energy minimisation was done at 0 K to reduce the overlapping of atoms. The systems were then slowly heated from 0 K to 350 K at a constant volume over 0.2 ns using a Langevin thermostat, with a damping parameter of 100 ps. Following equilibration in the NPT ensemble at 350 K and 1 atm, production runs were carried out in the NVT ensemble at 350 K to accelerate ion dynamics. A Nose–Hoover thermostat with a coupling constant of 200 fs for a duration of 150 ns. The time step was set at 1.5 fs. For subsequent analysis, trajectories were saved at 3 ps intervals. We conducted three independent simulations, each with unique initial conditions, to improve the reliability of our averaged results and estimation of error bars.

3 Results

3.1 Influence of fluorination on ion transport: insights from Onsager transport coefficients

MD simulations were performed to systematically investigate the impact of fluorinating diethyl ether-based solvents (F-DEEs) on ion transport, as illustrated in Fig. 1A and B. We evaluated the Onsager transport coefficients (F_{ij}), derived from simulation trajectories. Unlike the Nernst–Einstein equation, which assumes independent ion movement, the Onsager framework provides a quantitative measure for inter-ionic interactions and coupling between ionic fluxes. These coefficients thus offer a more comprehensive understanding by providing insights into the contributions of both self-diffusion and correlated ion motion to the overall transport properties.[34–37] Onsager coefficients (F_{ij}) were calculated using the following expressions:

$$F_{ij} = \frac{1}{6}\lim_{t\to\infty}\frac{d}{dt}\left\langle \sum_{\alpha}[\boldsymbol{r}_{i,\alpha}(t)-\boldsymbol{r}_{i,\alpha}(0)]\cdot\sum_{\beta}[\boldsymbol{r}_{j,\beta}(t)-\boldsymbol{r}_{j,\beta}(0)]\right\rangle \quad (1)$$

where, $\boldsymbol{r}_{i,\alpha}(t)$ represents the position of α^{th} particle of species i at time t with respect to the center of mass of the entire system. The angle brackets < … > denote averaging over different time origins and the number of particles so that these yield 'per-ion' transport coefficients. In the Onsager formalism, F_{ii}^{s} captures the self-motion of an ion while F_{ii}^{d} accounts for correlated motion with other ions of the same species. These are defined as:

$$F_{ii}^{d} = \frac{1}{6n_i}\lim_{t\to\infty}\frac{d}{dt}\left\langle \sum_{\alpha}\sum_{\beta\neq\alpha}[\boldsymbol{r}_{i,\alpha}(t)-\boldsymbol{r}_{i,\alpha}(0)]\cdot[\boldsymbol{r}_{i,\beta}(t)-\boldsymbol{r}_{i,\beta}(0)]\right\rangle \quad (2)$$

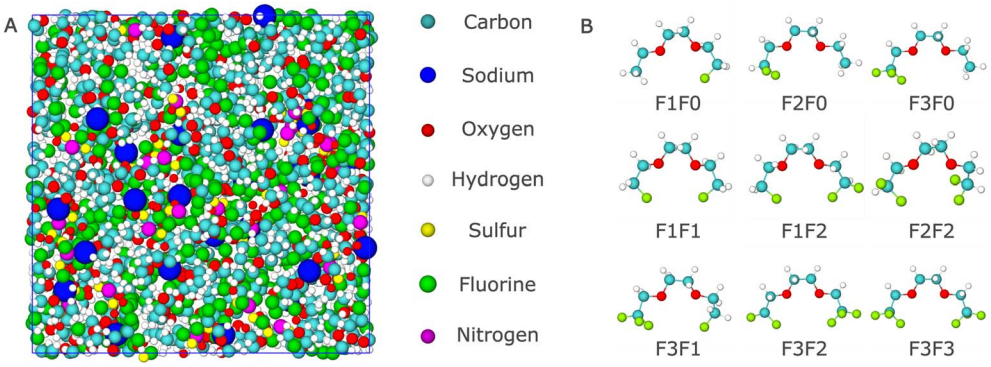

Fig. 1 Fluorinated DEEs (F-DEEs). (A) An equilibrated MD simulation snapshot of 1.0 M NaFSI in the F3F0 solvent. (B) A representative set of F-DEE molecules illustrating variations in unilateral and bilateral fluorine substitution of the diethyl ether (F0F0) molecule.

$$F_{ii}^{s} = \frac{1}{6n_i} \lim_{t\to\infty} \frac{d}{dt} \left\langle \sum_{\alpha} [r_{i,\alpha}(t) - r_{i,\alpha}(0)]^2 \right\rangle \quad (3)$$

Together, they reflect how much of an ion's displacement is due to its self-movement *versus* collective interactions. The transport coefficients are evaluated from the slope of mean square displacement terms (the expressions within < … > in eqn (1)–(3) where the log–log plot shows a slope equal to unity) (Fig. S1). Fig. 2A–C present the calculated Onsager coefficients (F_{ij}) for the various F-DEE systems. Fig. 2D provides a schematic illustration offering a physical picture of the transport coefficients F_{ij}. The self-correlation terms, F_{++}^{s} and F_{--}^{s}, which are proportional to the self-diffusion coefficients of cations and anions, respectively, exhibit a monotonic decrease with increasing fluorination (depicted by red bars in Fig. 2A and B). This trend suggests a reduction in the individual mobilities of both Na^+ and FSI^- ions as the degree of fluorination increases.

In contrast, the distinct terms, F_{++}^{d} and F_{--}^{d}, which quantify the correlated motion of like-ions, display a significant increase with fluorination (depicted by blue bars in Fig. 2A and B). Notably, these terms are negligible or negative in unfluorinated DEE and low-fluorinated DEEs (F1F0 and low-fluorinated bilaterally substituted F-DEEs), indicating anti-correlated

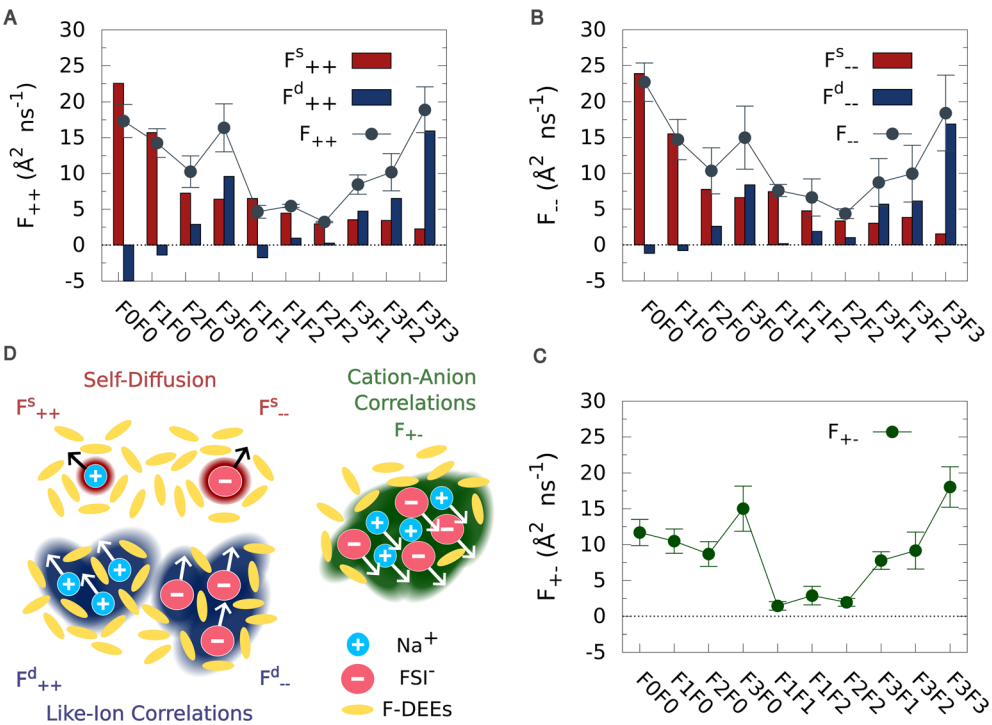

Fig. 2 Variation of Onsager transport coefficents with fluorination. Onsager transport coefficients for (A) cation–cation contributions from self terms F_{++}^{s} (red) and distinct terms F_{++}^{d} (blue). The overall $F_{++} = F_{++}^{s} + F_{++}^{d}$ coefficients are denoted by gray line points. (B) Anion–anion contributions from self-terms F_{--}^{s} (red), distinct terms F_{--}^{d} (blue). The overall $F_{--} = F_{--}^{s} + F_{--}^{d}$ coefficients are denoted by gray line points. (C) Cation–anion (F_{+-}) (green) correlated motions are shown across various F-DEE electrolytes. (D) A schematic depicting the physical significance of the various Onsager transport coefficients in the electrolytes. The standard deviations of F_{++}, F_{--}, F_{+-} are shown by the error bars.

motion of like-ions in these systems. However, in higher fluorinated, unilaterally and bilaterally substituted DEEs, F^d_{++} and F^d_{--} become significantly positive, signifying a strong positive correlation in motion of like-ions. For unilaterally substituted F-DEEs, the overall like–ion correlation coefficients (depicted by gray points in Fig. 2A and B) ($F_{++} = F^s_{++} + F^d_{++}$ and $F_{--} = F^s_{--} + F^d_{--}$) exhibit a near-parabolic dependence on the degree of fluorination, reflecting the competing contributions of the self and distinct terms.

The cation–anion correlated transport coefficients, represented by F_{+-}, are relatively low in the low-fluorinated bilaterally substituted F-DEEs (Fig. 2C). However, highly fluorinated systems, particularly the asymmetric F3F0 and the symmetric F3F3, exhibit significantly enhanced F_{+-} values. In the highly fluorinated bilaterally substituted F-DEEs, F_{+-} increases monotonically with the degree of fluorination, while the trends observed for F_{++} and F_{--} are roughly parabolic. We find that self-contributions to the Onsager coefficients (*e.g.*, F^s_{++}, F^s_{--}) exhibit low statistical uncertainty due to effective ensemble averaging. In contrast, distinct ion cross-correlation terms (*e.g.*, F^d_{++}, F^d_{--}, F_{+-}) display larger errors due to cross-correlation terms being inherently more sensitive to statistical noise.

These findings highlight the presence of significant ion–ion correlations in F-DEEs, which will have a critical role in determining the overall ionic conductivity of the electrolytes. Although increased fluorination reduces self-contribution to ion mobilities (as reflected in the variation of self-diffusion terms), it simultaneously promotes strong, positive correlations in the motion of like ions (distinct). F_{+-} in these systems further indicates that correlated cation–anion motion also plays a significant role. This suggests a transition to a transport regime in which correlated, potentially concerted, ion motion becomes a dominant contributor to conductivity, particularly in highly fluorinated DEEs.

3.2 Evaluating ionic conductivity (σ) beyond Nernst–Einstein: role of ion correlations

The ionic conductivity (σ), a critical parameter for electrolyte performance, was calculated from the Onsager coefficients. The expression for ionic conductivity σ, where the Onsager coefficients in the center-of-mass frame are used, is given by:

$$\sigma = \mathcal{F}^2\left(z_+{}^2 n_+ F_{++} + z_-{}^2 n_- F_{--} - 2 z_+ z_- n_- F_{+-}\right) \quad (4)$$

here, $\mathcal{F}$ is Faraday's constant, while F_{++}, F_{--}, and F_{+-} represent cation–cation, anion–anion, and cation–anion Onsager coefficients. z_+ and z_- denote the charges, and n_+ and n_- the total counts of Na^+ and FSI^-, respectively.

Fig. 3A presents the calculated ionic conductivities for the different F-DEE systems. The highest ionic conductivity is observed for the fully fluorinated F3F3 system, followed by the unilaterally substituted F-DEEs, with F3F0 exhibiting the highest conductivity. The low-fluorinated bilaterally substituted electrolytes display the lowest conductivities. This observation contrasts with the predictions based on the Nernst–Einstein equation, which neglects ion–ion correlations and predicts a monotonic decrease in conductivity with increasing fluorination (Fig. S2). This discrepancy highlights the importance of accounting for correlated ion motion, particularly ion pairing, in accurately determining ionic conductivity from molecular simulations.

These results are also in contrast to the generally observed trend of decreasing ionic conductivity with increasing fluorination reported for LIBs.[25,27,38] Yu *et al.* have experimentally measured the ionic conductivity of pure liquid Li-ion electrolytes without separators. 1.2 M LiFSI/F3F3 electrolyte has an ionic conductivity ~40% of that of unfluorinated 1.2 M LiFSI/F0F0.[22] To elucidate the contrasting behavior exhibited by Li^+ and Na^+, we conducted a parallel simulation using Li-ion salt while keeping all other parameters constant. Remarkably, our molecular dynamics simulations revealed a reduction in the ionic conductivity for Li^+ (Fig. S4), in agreement with experimental observations. Specifically, 1.0 M LiFSI/F3F3 exhibited an ionic conductivity of approximately 49% of that of the unfluorinated 1.0 M LiFSI/F0F0. This suggests that our simulations and methodology for computing ionic conductivity can capture behavior consistent with experiments and that the observed conductivity enhancement for Na^+ with fluorination is not a spurious outcome of the methodology.

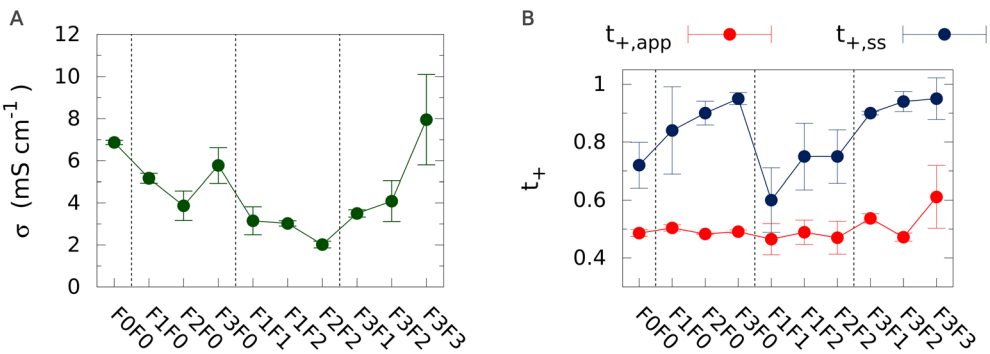

Fig. 3 Tuning ionic conductivity and transference numbers *via* fluorination. (A) Ionic conductivity (σ) (mS cm^{-1}) calculated from correlated diffusion coefficients of the charge carriers, *i.e.*, Na^+ and FSI^-. (B) Na^+ transference numbers (t_+) in various F-DEE electrolyte systems. The bars represent the standard deviations. The dashed lines categorize the F-DEEs into unfluorinated (F0F0), unilaterally substituted (F1F0, F2F0, F3F0), low-fluorinated bilaterally substituted (F1F1, F1F2, F2F2), and high-fluorinated bilaterally substituted (F3F1, F3F2, F3F3).

3.3 Ion correlation effects on Na^+ transference number (t_+)

The cation transference number (t_+), another crucial parameter for electrolyte performance, quantifies the fraction of current carried by the cation. To further understand the ion transport characteristics, we analyze the cation transference number using two distinct approaches: the apparent and the steady-state, both derived from Onsager transport coefficients obtained in the previous section. The apparent transference number (t_+^{app}), based on self-diffusion coefficients and the Nernst–Einstein approximation, provides a simplified estimate of Na^+ contribution to conductivity, serving as a baseline to assess the impact of neglecting ion correlations. t_+^{app} is often estimated experimentally using the pulsed-field gradient nuclear magnetic resonance (PFG-NMR) and potentiostatic polarization method.[39–41] The steady-state transference number (t_+^{ss}), computed from the full Onsager framework including cation–anion cross-correlations, reflects realistic transport behavior under electrochemical conditions, aligning with experimental metrics like those from Bruce-Vincent method and very-low-frequency (VLF) impedance spectroscopy.[42,43] Computing the two metrics helps us to comprehensively understand the transport mechanisms influenced by fluorination, from idealized dilute-like conditions to complex, correlation-dominated dynamics.

The apparent transference number, *i.e.*, t_+^{app} was estimated using the relation given below:

$$t_+^{app} = \frac{F^s_{++}}{F^s_{++} + F^s_{--}} \tag{5}$$

here F^s_{++} and F^s_{--} denote the self-diffusion coefficients of Na^+ and FSI^- respectively. t_+^{app} is approximately 0.5 for most F-DEEs, with a slight increase to 0.6 for F3F3 (Fig. 3B). This is due to the similar magnitudes of the self-diffusion coefficients for both cations and anions (Fig. 2A and B). However, this approach neglects ion–ion correlations and is only strictly valid in the infinite dilution limit, making it less accurate for electrolytes with significant ion pairing.

To account for ion–ion correlations, we also calculated the steady-state transference number, t_+^{ss}, using the theoretical framework developed by Shao *et al.*:[44]

$$t_+^{ss} = \frac{F^0_{++} - \frac{\left(F^0_{+-}\right)^2}{F^0_{--}}}{F^0_{++} + F^0_{--} - 2F^0_{+-}} \tag{6}$$

here, Onsager coefficients in the solvent frame of reference (F^0_{ij}) have been derived through the transformation relations given in eqn (S1)–(S3). The t_+^{ss} values increase with increasing fluorination in unilaterally substituted F-DEEs, reaching 0.95 for F3F0, compared to 0.72 in unfluorinated DEE (F0F0) (Fig. 3B). The low-fluorinated bilaterally fluorinated DEEs exhibit t_+^{ss} values between 0.6 and 0.75, while the high-fluorinated bilaterally fluorinated DEEs show enhanced t_+^{ss} values ranging from 0.90 to 0.95. Other works have also used fluorination of DME/DEE to get 1,1,1-trifluoro-2,3-dimethoxypropane (TFDMP)/bis(2-fluoroethyl) ethers (BFE) having improved transference numbers. The formation of aggregate clusters immobilizes FSI^- anions through coordination to realize high Li-ion transport and transference number in these electrolytes.[45,46]

3.4 Diffusion mechanisms: quantifying structural transport *via* the mixed transport coefficient

While ionic conductivity values provide a macroscopic assessment of ion transport, they do not inherently distinguish between the underlying microscopic mechanisms. Similarly, transference numbers alone offer limited insight into the manner in which ions migrate. In the present study of fluorinated DEE electrolytes, where we observe significant variations in both σ and t_+ with changing fluorination degree, a deeper understanding of the transport mechanism is crucial. Therefore, we employed the Mixed Transport Coefficient (MTC) to quantify the relative contributions of vehicular and structural diffusion. The MTC provides a critical link between the observed macroscopic transport properties and the microscopic dynamics of ion motion. This allows us to understand the conductivity and transference number trends in terms of the changing balance between structural diffusion and vehicular transport as a function of fluorination. The MTC is defined as:

$$\mathrm{MTC} = \frac{S}{V+S} = \frac{1}{N}\sum_{i=1}^{N}\left(\frac{\sum_{k=0}^{t_s}\Delta r_{i,k}{}^2}{\sum_{k=0}^{t_s}\Delta r_{i,k}{}^2 + \sum_{j=0}^{t_v}\Delta r_{i,j}{}^2}\right) \tag{7}$$

where N is the number of sodium ions, t_V is the cumulative time during which a sodium ion undergoes vehicular transport (*i.e.*, moves without exchanging solvent or anion neighbors in its first solvation shell), and t_S is the cumulative time during which a sodium ion exhibits structural transport (*i.e.*, undergoes hopping events involving solvent/anion exchange within the first solvation shell). $\Delta r_{i,k}$ and $\Delta r_{i,j}$ represent the displacements of the i^{th} sodium ion during time intervals corresponding to structural and vehicular transport, respectively.

Fig. 4A illustrates the calculated MTC values computed from 150 ns production trajectories of the various F-DEE-based electrolytes. A clear trend emerges: the MTC increases with the degree of fluorination, particularly in the highly fluorinated systems. This finding indicates a transition from a predominantly vehicular transport mechanism in the unfluorinated and low-fluorinated systems toward an increasing share of structural transport mechanism in the highly fluorinated DEEs.

Specifically, the MTC increases from 0.33 in unfluorinated DEE (F0F0) to 0.40 in F3F0, highlighting the growing importance of structural diffusion with increasing unilateral fluorination. The low-fluorinated bilaterally substituted DEEs exhibit relatively low MTC values, consistent with a predominantly vehicular transport mechanism, likely due to their stronger solvation energies.[24] However, in the highly fluorinated bilaterally substituted DEEs, the MTC continues to rise, reaching 0.45 in F3F3. Fig. 4B presents the mode-time markers for a representative Na^+ ion in two electrolytes: F0F0 and F3F0. For visual clarity, the mode-time markers are shown over a 15 ns segment. The ion alternates between vehicular (V) and

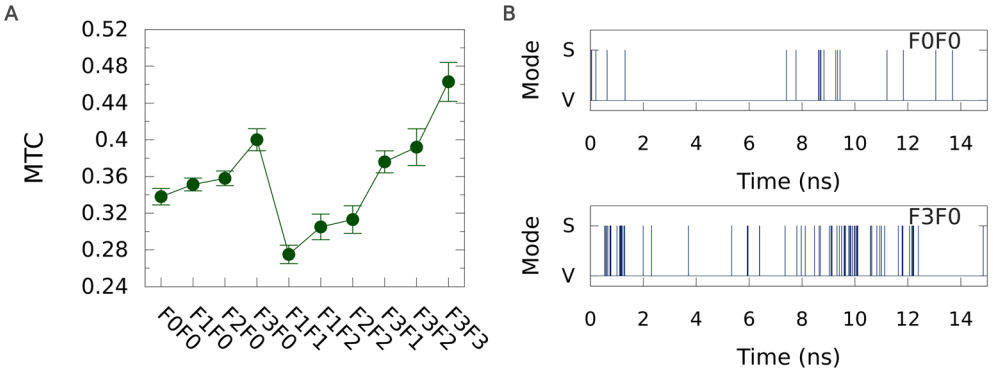

Fig. 4 Characterizing Na^+ transport modes in F-DEEs *via* Mixed Transport Coefficient. (A) Mixed Transport Coefficient (MTC) illustrating the extent of structural transport contributions to Na^+ mobility across various F-DEE-based electrolytes. (B) Mode-time markers of a representative Na^+ ion in two electrolytes—F0F0 (top) and F3F0 (bottom)—highlighting periods of structural (S) *versus* vehicular (V) transport modes.

structural (S) transport modes over time. Notably, F0F0 predominantly exhibits vehicular transport, while the higher frequency of jumps in F3F0 (bottom panel) highlights a greater contribution from structural transport in this fluorinated system.

The observed trend of increasing MTC with fluorination, coupled with the positive values of F^d_{++} and F^d_{--} (Fig. 2A and B), provides strong evidence for a concerted hopping mechanism in the highly fluorinated systems. This mechanism resembles the Grotthuss mechanism observed in proton transport, where the hopping of one Na^+ ion into a new coordination site induces the displacement of the previously occupying Na^+ ion to the next coordination site. This concerted motion of ions, particularly within aggregates in low-dielectric-constant/high-donor-number environments, contributes significantly to the enhanced ionic conductivity and transference numbers observed in these systems.[47–49]

3.5 Solvation shell structure

To understand the molecular origins of highly fluorinated solvents preferring structural relaxations as compared to low-fluorinated solvent, we investigated the solvation shell structure around sodium ions. Table 1 provides a quantitative analysis of the first solvation shell composition, detailing the populations of various combinations of FSI^- and F-DEE solvent molecules within the primary coordination sphere of Na^+.

In F0F0, the solvation environment is dominated by solvent molecules, with 31% of solvation shells containing three DEE molecules and a significant fraction also containing two DEE and one FSI^- molecule. This prevalence of solvent-rich solvation shells classifies F0F0 as a strong solvating solvent.[22,25]

In the unilaterally substituted F-DEEs, solvent-only solvation shells are absent. With increasing fluorination, FSI^- gradually replaces solvent molecules in the solvation shell, as evidenced by the monotonic increase in the Na^+-OFSI coordination number (Fig. S2). This substitution process leads to a decrease in single Na^+-anion pair (1FSI, 2DEE) structures and an increase in Na^+-anion clustered solvation shells (> = 2FSI). Notably, F3F0 exhibits a significant population (32%) of four-molecule-coordinated solvation shells, specifically the (3FSI, 1F-DEE) configuration. Additionally, four-molecule-coordinated solvation shells containing two FSI and two F-DEE are also present and their population increases with the degree of fluorination, reaching 21% in F3F0. The presence of these larger, four-molecule-coordinated solvation shells in F3F0 is directly linked to the transition from a predominantly vehicular to a mixed vehicular-structural transport mechanism, resulting in enhanced ionic conductivity and transference number.

In contrast, the low-fluorinated bilaterally substituted F-DEEs, particularly F1F1, are characterized by a significant population of solvent-separated ion pairs. For example, nearly 50% of the solvation shells in F1F1 contain only two solvent

Table 1 Distribution of Na^+ solvation shells, where nFSI^- and nF-DEE represent the number of FSI^- anions and F-DEE molecules, respectively, inside the solvation shell. The dominant solvation structures for each F-DEE system are highlighted in bold

($nFSI^-$, nF-DEE)	F0F0	F1F0	F2F0	F3F0	F1F1	F1F2	F2F2	F3F1	F3F2	F3F3
(0,3)	**31.90**	2.94	0.75	0.10	0.55	0.19	0.08	0.05	0.04	0.00
(0,2)	0.12	2.77	0.89	0.03	**44.84**	**28.49**	**21.26**	3.64	2.44	0.01
(1,2)	**60.02**	**76.71**	**56.14**	**26.51**	**40.54**	**35.34**	**32.02**	**30.43**	**20.68**	2.69
(2,1)	1.59	8.65	**15.73**	16.51	10.22	**24.36**	**30.67**	**33.27**	**34.11**	**18.33**
(2,2)	5.39	6.81	**15.31**	**21.02**	1.58	3.51	3.30	6.78	5.68	3.37
(3,1)	0.51	1.83	10.58	**32.00**	1.95	7.28	11.63	**23.13**	**30.08**	**45.58**
(4,0)	0.01	0.03	0.04	1.09	0.00	0.03	0.32	1.04	2.83	9.52
(4,1)	0.00	0.01	0.18	1.55	0.02	0.03	0.08	0.38	1.68	7.54

molecules. The high Na^+-FDEE coordination numbers in these systems further support the prevalence of solvent-dominated solvation environments (Fig. S3). As fluorination increases in the low-fluorinated bilaterally substituted F-DEEs, the population of three-molecule solvation shells (2FSI, 1F-DEE) initially rises and then declines, while the population of solvent-only shells decreases. However, clustered solvation shells remain relatively insignificant. These observations along with low MTC values suggest that in solvent-dominated solvation environments, found in low-fluorinated bilaterally substituted F-DEEs, Na^+ ions diffuse primarily *via* the vehicular mechanism, with the solvent-solvated sodium complexes moving independently. The low ionic conductivity of these systems, despite the presence of solvent-separated ion pairs, contradicts the conventional expectation that such species facilitate faster sodium diffusion in dilute electrolytes.[50–53]

In the highly fluorinated bilaterally substituted F-DEEs, anion-clustered solvation complexes become dominant. With increasing fluorination, the population of four-molecule-coordinated solvation shells grows substantially. In F3F3, over 60% of the cation solvation shells are highly aggregated, with 46% comprising four molecules. These aggregates predominantly consist of anion-rich configurations, such as (3FSI, 1DEE), where an anion is coordinated to multiple sodium ions. The increasing Na^+-OFSI coordination number in the bilaterally substituted F-DEEs (Fig. S3) further corroborates this trend towards aggregation. Bilateral low fluorination of DEE enhances Na^+ coordination *via* localized Na–F interactions, while reducing electron density on ether oxygens and tuning solvation strength. However, excessive fluorination causes charge delocalization, weakening Na^+–solvent binding.[22,24,25] This results in a shift from solvent-dominated to anion-rich solvation shells, facilitating faster ligand exchange and promoting structural diffusion mechanisms. In low bilaterally-substituted F-DEE solvents, vehicular motion dominates due to strong solvent coordination, while in highly fluorinated solvents, weak Na^+–solvent interactions enable dynamic ligand rearrangements and enhanced ionic mobility.

The partial radial distribution functions (pRDFs) of Li^+ with the oxygen atoms of both FSI^- and F-DEEs exhibit a clear shift of ~0.36 Å toward shorter distances compared to Na^+, along with sharper and narrower peaks, as shown in Fig. S5. These features indicate that Li^+ forms more compact and strongly bound solvation shells. Moreover, the RDF peak height increases significantly with fluorination (F0F0 to F3F3), suggesting that more anions enter the Li^+ solvation shell, promoting persistent ion-pairing. These features collectively point to significantly stronger ion–solvent and ion–anion interactions for Li^+. As a result, Li^+ forms tightly bound solvation environments, which persist over longer timescales and hinder its mobility relative to Na^+. Furthermore, the ionic conductivity in the Li-based electrolytes followed the trend ($-CH_2F > -CH_3 > -CHF_2 > -CF_3$) of β-fluorination in DEEs.[22,23] This is contrasting to the Na-ion in F-DEEs where the polar and strongly interacting groups $-CH_2F$ and $-CHF_2$ groups tend to have lower ionic conductivities as in the case of low bilaterally substituted F-DEEs. This contrast may arise from the weaker Na–F interactions relative to Li–F. In Li^+ electrolytes, stronger ion–solvent interactions promote vehicular diffusion, whereas in Na^+ systems, stronger solvation in low bilaterally substituted F-DEEs compared to unfluorinated DEE suppresses structural diffusion, resulting in lower conductivities.

The observation of enhanced ionic conductivity and transference numbers in highly fluorinated DEE electrolytes, simultaneous with the prevalence of multi-anion, cluster-like solvation shells around the Na^+ cation (*e.g.*, (3FSI, 1F-DEE)), presents a counterintuitive result. Conventionally, increased fluorination and the formation of such ionic aggregates are associated with reduced ionic conductivity, owing to the decreased mobility of larger, less-charged species. However, our calculated MTC values for these highly fluorinated systems indicate a dominance of structural diffusion over vehicular transport. This suggests a paradigm shift: the key to understanding this enhanced transport lies not solely in the static solvation structure, but in its dynamics. We hypothesize that these distinct solvation environments, characterized by varying numbers and arrangements of anions and solvent molecules, possess a spectrum of relaxation timescales. Particularly, the total solvation number of the species inside the Na^+ solvation shell plays a crucial role in determining the lifetime of the solvation shell. The presence of faster relaxation modes, facilitated by rapid anion and solvent exchange kinetics within these clusters, could enable a highly efficient Grotthuss-like hopping mechanism, overcoming the limitations typically imposed by aggregate formation *via* the Stokes–Einstein relation. To rigorously test this hypothesis and quantify the dynamics of these critical solvation structures, we performed detailed analyses of solvation shell lifetimes and relaxation processes, as presented in the following section.

3.6 Solvation shell dynamics: lifetimes and relaxation processes

To understand the role of solvation shell structure on the relaxation modes, we investigated the lifetimes/lifetimes of the different primary solvation shell configurations of Na^+. A geometric criterion, *e.g.* neighbor variable $H(r,t)$, is defined as equal unity if the distance between the Na^+ and the oxygens of a certain species (F-DEE or FSI^-) is within a specified cutoff at a certain time t. We have chosen the distance cutoff as the first minimum of the corresponding pRDFs to encompass the first solvation shell. From this, the neighbor autocorrelation function (NACF) for a particular solvation configuration having x FSI^- and y F-DEE is calculated using

$$\mathrm{NACF}_{(x\mathrm{FSI}^-,y\mathrm{F\text{-}DEE})}(t) = \frac{\sum \langle H(\tau_0 + t)H(\tau_0)\rangle}{\sum \langle H(0)H(0)\rangle}, \quad (8)$$

where t is the correlation time and $< \ldots >$ depicts the time-origin averaging done through the initial frames τ_0 and the total number of Na^+. Since reformation is not allowed, these are called continuous NACFs.[51,54] These NACFs were fitted with a single exponential that provides insights into the lifetimes (τ) of survival of these solvation cages. Fig. 5 shows the lifetimes and percentages of the solvation shells for different F-DEE

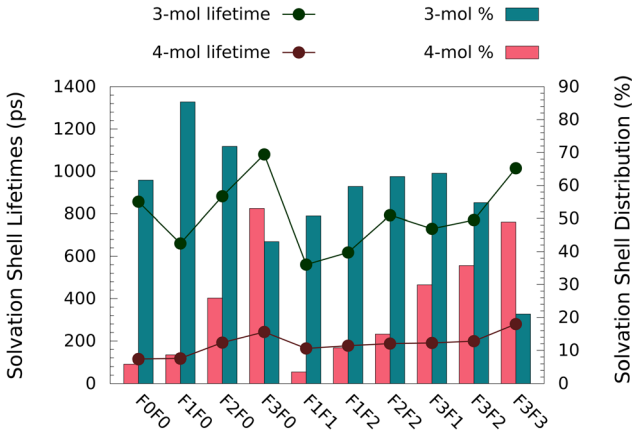

Fig. 5 Solvation shell lifetimes. Left axis: lifetimes (in ps) of three-molecule solvation shells (2 FSI, 1 F-DEE or 2 F-DEE, 1 FSI) shown as green-colored points, and four-molecule shells (2 F-DEE, 2 FSI or 3 FSI, 1 F-DEE) shown as red-colored points across different F-DEE electrolytes. Right axis: fraction of three-molecule solvation shells (2 FSI, 1 F-DEE or 2 F-DEE, 1 FSI) and four-molecule solvation shells (2 F-DEE, 2 FSI or 3 FSI, 1 F-DEE) depicted by colored bars.

electrolytes. The average lifetimes of solvation shells containing three coordinated/solvated molecules (2 FSI, 1 F-DEE or 1 F-DEE, 2 FSI) and four coordinated molecules (3 FSI, 1 F-DEE or 2 FSI, 2 F-DEE) are depicted in the figure. Four-molecule solvation shells show increasing lifetimes with fluorination, rising from 68.1 ps in F0F0 to 339 ps in F3F3, peaking at 251.3 ps in F3F0 among unilaterally fluorinated systems. Similarly, three-molecule solvation shells exhibit increases in lifetime with fluorination, with F3F0 showing the highest values across all systems. Notably, solvation shells containing four molecules exhibit significantly faster relaxation dynamics (approximately three to four times faster) compared to three-molecule solvation shells.

The overall transport of Na^+ ions is influenced by both the solvation number of their primary solvation shells and the relative presence of each solvation configuration. As discussed in the previous section, with increasing fluorination-whether unilaterally or bilaterally—the proportion of four-molecule solvation shells grows compared to three-molecule shells (Fig. 5). In highly fluorinated DEEs, such as F3F0 and F3F3, four-molecule solvation shells become more dominant than the three-molecule ones. The combination of short lifetimes and high populations of four-molecule solvation shells in F3F0 and other highly fluorinated, bilaterally substituted F-DEEs promotes a transition toward a structural diffusion mechanism. These differences in solvation shell lifetimes likely reflect variations in the free energy landscape, where FSI^--rich environments (*e.g.*, 3 FSI^-, 1 F3F3) offer shallower free-energy minimum and lower transition barriers. Similar trends have been reported in free-energy analyses in previous works.[55,56] The flexible, weakly coordinating nature of FSI^- facilitates rapid ligand exchange and enables efficient structural ion transport *via* dynamic ion rearrangements.

Further insights into the solvation shell dynamics were obtained by calculating the Neighbor autocorrelation functions (NACFs) of the Na^+–O bonds for both anions and solvent molecules within all solvation shells (Fig. S6 and S7). These ACFs provide information about the average time a particular species (FSI^- or F-DEE) remains within the first solvation shell of Na^+.

The bi-exponential fitting of the neighbor ACFs for Na^+–O_{FSI} bonds reveals relaxation modes in the range of 0–1 ns (Fig. S6). These relaxation times are significantly faster than those of the Na^+–O_{F-DEE} bonds, which range from 4.5–25 ns. This indicates that the dominant contribution to structural motion arises from the fast relaxation modes of the Na^+–O_{FSI} bonds within the solvation shells. The $\tau_{Na^+-O_{FSI}}$ values increase with increasing fluorination (Fig. S6A and B). On the other hand, the solvent lifetimes ($\tau_{Na^+-O_{F\text{-}DEE}}$) decrease with increasing fluorination (Fig. S7). Thus, the solvent relaxation becomes faster in the anion-rich, clustered solvation shells prevalent in the highly fluorinated systems. This is consistent with the weakened interaction between Na^+ and the highly fluorinated terminal ends of the F-DEE solvent molecules, facilitating faster solvent exchange and promoting structural diffusion.[24] These rapid solvent/anion exchanges, particularly within the four-molecule-coordinated solvation shells in F3F0 and highly fluorinated bilaterally substituted F-DEEs are key factors contributing to the enhanced ionic conductivity and transference numbers *via* the promotion of a rapid ion-hopping mechanism.

The solvation shell compositions of Li^+ and Na^+ in F3F3 are broadly similar in terms of dominant configurations (*e.g.*, 3 FSI^- and 1 DEE), but the dynamics differ significantly. Li^+-containing aggregates exhibit residence times nearly twice as long as their Na^+ counterparts, indicating more stable and less dynamic solvation structures. For 3-molecule shells (2 FSI^-, 1 F3F3), the residence time for Li^+ is nearly four times longer than for Na^+, further reducing its mobility. This difference in solvation dynamics underpins the higher conductivity observed in NaFSI/F3F3 compared to LiFSI/F3F3. Furthermore, Li^+ exhibits only a moderate increase in MTC (0.29 to 0.36) from F0F0 to F3F3, reflecting limited enhancement in structural diffusion. These observations stem from fundamental differences in the ionic properties of Li^+ and Na^+. Li^+, with its smaller ionic radius and higher charge density, forms stronger electrostatic interactions with both anions and solvents, resulting in tightly bound solvation shells. In contrast, larger size and lower charge density of Na^+ lead to weaker interactions and more flexible coordination environments, enabling faster solvation shell rearrangements and enhanced structural diffusion.

4 Discussion and conclusion

We have systematically investigated the influence of terminal fluorination in DEE-based electrolytes on the solvation structure, dynamics, and ion transport properties in SIBs. By employing all-atom MD simulations and analyzing the results within the framework of Onsager transport coefficients and the mixed transport coefficient, we have shown a fundamental shift in the dominant ion transport mechanism from predominantly

vehicular to a mixed vehicular-structural with an increasing degree of fluorination.

In unfluorinated DEE and low-fluorinated analogs, Na^+ transport is primarily governed by the vehicular mechanism, where the ion migrates along with its intact, solvent-dominated solvation shell. This is supported by the prevalence of solvent-separated ion pairs, the low MTC values, and the relatively long lifetimes of solvent molecules within the solvation shell. However, as the degree of fluorination increases, particularly in the highly fluorinated unilaterally substituted (F3F0) and bilaterally substituted (F3F3) F-DEEs, a distinct transition towards a structural transport mechanism is observed.

This transition is driven by several key factors. First, fluorination significantly alters the composition of the Na^+ solvation shell. While unfluorinated DEE favors solvation environments rich in solvent molecules, highly fluorinated DEEs promote the formation of anion-clustered solvation shells, particularly four-molecule coordinated configurations like (3FSI, 1F-DEE) and (2FSI, 2F-DEE). Second, these anion-rich solvation shells exhibit significantly faster relaxation dynamics, as evidenced by the shorter lifetimes of both solvent and anion species within the shell. This accelerated structural relaxation facilitates more frequent solvent/anion exchange events, promoting a Grotthuss-like hopping mechanism for Na^+ transport. Third, the increasing contribution of structural diffusion is further corroborated by the substantial increase in the MTC with increasing fluorination, reaching values as high as 0.45 in F3F3. Finally, the positive values of the distinct Onsager coefficients (F^d_{++} and F^d_{--}) in the highly fluorinated systems indicate a concerted hopping mechanism, where the movement of one Na^+ ion into a new coordination site triggers the displacement of another Na^+ ion, leading to enhanced, correlated ion motion.

The observed enhancement in structural diffusion in the highly fluorinated DEEs has profound implications for the overall ion transport properties. Notably, F3F0 and F3F3 exhibit higher ionic conductivities and Na^+ transference numbers compared to their unfluorinated or less fluorinated counterparts. This finding challenges the conventional notion that ion pairing and aggregation, which are more prevalent in the highly fluorinated systems as evidenced by the solvation shell analysis, universally hinder ion transport. Instead, our results demonstrate that when ion aggregation is coupled with fast structural relaxation and a shift towards structural diffusion, it can lead to improved transport properties. Despite FSI^--rich solvation and stronger Na^+–FSI^- correlations in F3F3, these are short-lived, indicating rapid ligand exchange dynamics. This is in contrast to Li-ion studies where ion pairing is understood to impede ion transport due to the formation of large, immobile aggregates that cannot contribute to structural diffusion and lower the fraction of free ions that can take part in vehicular transport.

The insights gained from this study have significant implications for the design of high-performance electrolytes for SIBs. By strategically introducing fluorine atoms into solvent molecules, it is possible to manipulate the solvation environment and promote structural diffusion, leading to enhanced ionic conductivity and transference numbers. This approach offers a promising alternative to conventional electrolyte design strategies that primarily rely on optimizing salt concentration to enhance vehicular transport.

However, it is important to acknowledge that the optimal degree of fluorination may depend on a delicate balance between promoting structural diffusion and avoiding excessive ion pairing that could ultimately hinder ion transport. While F3F0 and F3F3 demonstrate superior transport properties in this study, further investigations are needed to explore the effects of even higher degrees of fluorination and different fluorination patterns. Additionally, the influence of salt type, salt concentration, and temperature on the solvation structure, dynamics, and ion transport mechanisms in F-DEE-based electrolytes warrants further investigation.

In conclusion, this work provides a fundamental understanding of the role of fluorination in modulating ion transport mechanisms in liquid electrolytes. The demonstrated ability to promote structural diffusion through strategic fluorination opens up new avenues for the design of advanced electrolytes for next-generation SIBs and other electrochemical energy storage devices. By combining computational modeling with experimental validation, it will be possible to develop a more complete understanding of ion transport phenomena in complex electrolyte systems and to design electrolytes that can meet the demanding requirements of future energy storage applications.

Conflicts of interest

There are no conflicts to declare.

Data availability

The data supporting this article have been included as part of the SI (Tables S1 and S2, Fig. S1–S7, eqn (S1)–(S3). See DOI: **https://doi.org/10.1039/d5ta04224k**.

Acknowledgements

The authors would like to thank the Department of Science and Technology (DST), India for the grant under the project "DST-Integrated Clean Energy Material Acceleration Platform (IC-MAP) on storage." S. K. B. acknowledges the scholarship granted by the Ministry of Education (formerly MHRD) through the Indian Institute of Technology Bhubaneswar (IIT Bhubaneswar).

References

1 Z. Tian, Y. Zou, G. Liu, Y. Wang, J. Yin, J. Ming and H. N. Alshareef, *Advanced Science*, 2022, **9**, 2201207.
2 Y. Liu, Y. Zhu and Y. Cui, *Nat. Energy*, 2019, **4**, 540–550.
3 M. Li, C. Wang, Z. Chen, K. Xu and J. Lu, *Chem. Rev.*, 2020, **120**, 6783–6819.
4 Y. S. Meng, V. Srinivasan and K. Xu, *Science*, 2022, **378**, eabq3750.
5 N. Yao, X. Chen, Z.-H. Fu and Q. Zhang, *Chem. Rev.*, 2022, **122**, 10970–11021.

6 N. Yao, L. Yu, Z.-H. Fu, X. Shen, T.-Z. Hou, X. Liu, Y.-C. Gao, R. Zhang, C.-Z. Zhao, X. Chen, *et al.*, *Angew. Chem.*, 2023, **135**, e202305331.
7 K.-D. Kreuer, A. Rabenau and W. Weppner, *Angew Chem. Int. Ed. Engl.*, 1982, **21**, 208–209.
8 D. J. Siegel, L. Nazar, Y.-M. Chiang, C. Fang and N. P. Balsara, *Trends Chem.*, 2021, **3**, 807–818.
9 E. Crabb, A. Aggarwal, R. Stephens, Y. Shao-Horn, G. Leverick and J. C. Grossman, *J. Phys. Chem. B*, 2024, **128**, 3427–3441.
10 T. Hou, K. D. Fong, J. Wang and K. A. Persson, *Chem. Sci.*, 2021, **12**, 14740–14751.
11 K. Dokko, D. Watanabe, Y. Ugata, M. L. Thomas, S. Tsuzuki, W. Shinoda, K. Hashimoto, K. Ueno, Y. Umebayashi and M. Watanabe, *J. Phys. Chem. B*, 2018, **122**, 10736–10745.
12 N. Agmon, *Chem. Phys. Lett.*, 1995, **244**, 456–462.
13 M. Wu, X. Liu, H. Liu, D. Li, X. Qi, J. Zeng, L. Gao, C.-W. Nan and L.-Z. Fan, *Nat. Commun.*, 2025, **16**, 2808.
14 D. Lu, R. Li, M. M. Rahman, P. Yu, L. Lv, S. Yang, Y. Huang, C. Sun, S. Zhang, H. Zhang, J. Zhang, X. Xiao, T. Deng, L. Fan, L. Chen, J. Wang, E. Hu, C. Wang and X. Fan, *Nature*, 2024, **627**, 101–107.
15 A. B. Faheem, T. D. Pham and K.-K. Lee, *J. Mol. Liq.*, 2024, **415**, 126344.
16 J. Self, K. D. Fong and K. A. Persson, *ACS Energy Lett.*, 2019, **4**, 2843–2849.
17 H. K. Bergstrom and B. D. McCloskey, *ACS Energy Lett.*, 2024, **9**, 373–380.
18 O. Borodin, L. Suo, M. Gobet, X. Ren, F. Wang, A. Faraone, J. Peng, M. Olguin, M. Schroeder, M. S. Ding, E. Gobrogge, A. von Wald Cresce, S. Munoz, J. A. Dura, S. Greenbaum, C. Wang and K. Xu, *ACS Nano*, 2017, **11**, 10462–10471.
19 O. Borodin, J. Self, K. A. Persson, C. Wang and K. Xu, *Joule*, 2020, **4**, 69–100.
20 N. Von Aspern, G.-V. Röschenthaler, M. Winter and I. Cekic-Laskovic, *Angew. Chem., Int. Ed.*, 2019, **58**, 15978–16000.
21 C. V. Amanchukwu, Z. Yu, X. Kong, J. Qin, Y. Cui and Z. Bao, *J. Am. Chem. Soc.*, 2020, **142**, 7393–7403.
22 Z. Yu, P. E. Rudnicki, Z. Zhang, Z. Huang, H. Celik, S. T. Oyakhire, Y. Chen, X. Kong, S. C. Kim, X. Xiao, H. Wang, Y. Zheng, G. A. Kamat, M. S. Kim, S. F. Bent, J. Qin, Y. Cui and Z. Bao, *Nat. Energy*, 2022, **7**, 94–106.
23 Y. Lin, Z. Yu, W. Yu, S.-L. Liao, E. Zhang, X. Guo, Z. Huang, Y. Chen, J. Qin, Y. Cui, *et al.*, *J. Mater. Chem. A*, 2024, **12**, 2986–2993.
24 S. K. Barik, S. Das Adhikari and H. Kumar, *ACS Appl. Energy Mater.*, 2025, **8**, 7673–7683.
25 X. Yuan, X. Chen, Y. Zhou, Z. Yu and X. Kong, *J. Energy Chem.*, 2025, **102**, 52–62.
26 Y. Chen, Z. Yu, P. Rudnicki, H. Gong, Z. Huang, S. C. Kim, J.-C. Lai, X. Kong, J. Qin, Y. Cui, *et al.*, *J. Am. Chem. Soc.*, 2021, **143**, 18703–18713.
27 X. Yuan, L. Du, J. Li, Z. Liu, D. Lu and X. Kong, *J. Phys.: Condens. Matter*, 2024, **36**, 235101.
28 A. P. Thompson, H. M. Aktulga, R. Berger, D. S. Bolintineanu, W. M. Brown, P. S. Crozier, P. J. In't Veld, A. Kohlmeyer, S. G. Moore, T. D. Nguyen, *et al.*, *Comput. Phys. Commun.*, 2022, **271**, 108171.
29 L. S. Dodda, I. Cabeza de Vaca, J. Tirado-Rives and W. L. Jorgensen, *Nucleic Acids Res.*, 2017, **45**, W331–W336.
30 M. J. Frisch, G. W. Trucks, H. B. Schlegel, G. E. Scuseria, M. A. Robb, J. R. Cheeseman, G. Scalmani, V. Barone, G. A. Petersson, H. Nakatsuji, X. Li, M. Caricato, A. V. Marenich, J. Bloino, B. G. Janesko, R. Gomperts, B. Mennucci, H. P. Hratchian, J. V. Ortiz, A. F. Izmaylov, J. L. Sonnenberg, D. Williams-Young, F. Ding, F. Lipparini, F. Egidi, J. Goings, B. Peng, A. Petrone, T. Henderson, D. Ranasinghe, V. G. Zakrzewski, J. Gao, N. Rega, G. Zheng, W. Liang, M. Hada, M. Ehara, K. Toyota, R. Fukuda, J. Hasegawa, M. Ishida, T. Nakajima, Y. Honda, O. Kitao, H. Nakai, T. Vreven, K. Throssell, J. A. Montgomery, Jr., J. E. Peralta, F. Ogliaro, M. J. Bearpark, J. J. Heyd, E. N. Brothers, K. N. Kudin, V. N. Staroverov, T. A. Keith, R. Kobayashi, J. Normand, K. Raghavachari, A. P. Rendell, J. C. Burant, S. S. Iyengar, J. Tomasi, M. Cossi, J. M. Millam, M. Klene, C. Adamo, R. Cammi, J. W. Ochterski, R. L. Martin, K. Morokuma, O. Farkas, J. B. Foresman and D. J. Fox, *Gaussiañ16 Revision C.01*, Gaussian Inc. Wallingford CT., 2016.
31 A. S. Gouveia, C. E. Bernardes, L. C. Tomé, E. I. Lozinskaya, Y. S. Vygodskii, A. S. Shaplov, J. N. C. Lopes and I. M. Marrucho, *Phys. Chem. Chem. Phys.*, 2017, **19**, 29617–29624.
32 L. Martínez, R. Andrade, E. G. Birgin and J. M. Martínez, *J. Comput. Chem.*, 2009, **30**, 2157–2164.
33 J.-P. Ryckaert, G. Ciccotti and H. J. Berendsen, *J. Comput. Phys.*, 1977, **23**, 327–341.
34 K. D. Fong, H. K. Bergstrom, B. D. McCloskey and K. K. Mandadapu, *AIChE J.*, 2020, **66**, e17091.
35 K. D. Fong, J. Self, B. D. McCloskey and K. A. Persson, *Macromolecules*, 2021, **54**, 2575–2591.
36 C. Fang, A. Mistry, V. Srinivasan, N. P. Balsara and R. Wang, *JACS Au*, 2023, **3**, 306–315.
37 A. France-Lanord and J. C. Grossman, *Phys. Rev. Lett.*, 2019, **122**, 136001.
38 Y. Lin, Z. Yu, W. Yu, S.-L. Liao, E. Zhang, X. Guo, Z. Huang, Y. Chen, J. Qin, Y. Cui and Z. Bao, *J. Mater. Chem. A*, 2024, **12**, 2986–2993.
39 Y. Yin, Y. Yang, D. Cheng, M. Mayer, J. Holoubek, W. Li, G. Raghavendran, A. Liu, B. Lu, D. M. Davies, Z. Chen, O. Borodin and Y. S. Meng, *Nat. Energy*, 2022, **7**, 548–559.
40 J. Evans, C. A. Vincent and P. G. Bruce, *Polymer*, 1987, **28**, 2324–2328.
41 J. Xu, J. Zhang, T. P. Pollard, Q. Li, S. Tan, S. Hou, H. Wan, F. Chen, H. He, E. Hu, K. Xu, X.-Q. Yang, O. Borodin and C. Wang, *Nature*, 2023, **614**, 694–700.
42 P. G. Bruce and C. A. Vincent, *J. Electroanal. Chem. Interfacial Electrochem.*, 1987, **225**, 1–17.
43 Y. Shao, H. Gudla, J. Mindemark, D. Brandell and C. Zhang, *Acc. Chem. Res.*, 2024, **57**, 1123–1134.
44 Y. Shao and C. Zhang, *J. Chem. Phys.*, 2023, **158**, 161104.
45 G. Zhang, J. Chang, L. Wang, J. Li, C. Wang, R. Wang, G. Shi, K. Yu, W. Huang, H. Zheng, *et al.*, *Nat. Commun.*, 2023, **14**, 1081.

46 Y. Zhao, T. Zhou, M. Mensi, J. W. Choi and A. Coskun, *Nat. Commun.*, 2023, **14**, 299.
47 X. Wu, J. J. Hong, W. Shin, L. Ma, T. Liu, X. Bi, Y. Yuan, Y. Qi, T. W. Surta, W. Huang, J. Neuefeind, T. Wu, P. A. Greaney, J. Lu and X. Ji, *Nat. Energy*, 2019, **4**, 123–130.
48 X. He, Y. Zhu and Y. Mo, *Nat. Commun.*, 2017, **8**, 15893.
49 Y. Watanabe, Y. Ugata, K. Ueno, M. Watanabe and K. Dokko, *Phys. Chem. Chem. Phys.*, 2023, **25**, 3092–3099.
50 O. Borodin and G. Smith, *J. Solution Chem.*, 2007, **36**, 803–813.
51 T. P. Liyana-Arachchi, J. B. Haskins, C. M. Burke, K. M. Diederichsen, B. D. McCloskey and J. W. Lawson, *J. Phys. Chem. B*, 2018, **122**, 8548–8559.
52 X. Chen, Z. Li, H. Zhao, J. Li, W. Li, C. Han, Y. Zhang, L. Lu, J. Li and X. Qiu, *ACS Nano*, 2024, **18**, 8350–8359.
53 Y. Yamada, J. Wang, S. Ko, E. Watanabe and A. Yamada, *Nat. Energy*, 2019, **4**, 269–280.
54 M. Brehm and D. Sebastiani, *J. Chem. Phys.*, 2018, **148**, year.
55 A. Baskin and D. Prendergast, *J. Phys. Chem. Lett.*, 2020, **11**, 9336–9343.
56 A. Aggarwal, K. Gordiz, A. Baskin, D. Vivona, J. Halldin Stenlid, J. W. Lawson, J. C. Grossman and Y. Shao-Horn, *J. Phys. Chem. C*, 2024, **128**, 12903–12915.

